Zero-Shot Event-Intensity Asymmetric Stereo via Visual Prompting from Image Domain

Hanyue Lou[#1,2] **Jinxiu Liang**[#1,2] **Minggui Teng**[1,2] **Bin Fan**[3] **Yong Xu**[4] **Boxin Shi**[*1,2]
[1] State Key Laboratory of Multimedia Information Processing, School of Computer Science, Peking University
[2] National Engineering Research Center of Visual Technology, School of Computer Science, Peking University
[3] National Key Laboratory of General AI, School of Intelligence Science and Technology, Peking University
[4] School of Computer Science and Engineering, South China University of Technology
{hylz,cssherryliang,minggui_teng,binfan,shiboxin}@pku.edu.cn yxu@scut.edu.cn

Abstract

Event-intensity asymmetric stereo systems have emerged as a promising approach for robust 3D perception in dynamic and challenging environments by integrating event cameras with frame-based sensors in different views. However, existing methods often suffer from overfitting and poor generalization due to limited dataset sizes and lack of scene diversity in the event domain. To address these issues, we propose a zero-shot framework that utilizes monocular depth estimation and stereo matching models pretrained on diverse image datasets. Our approach introduces a visual prompting technique to align the representations of frames and events, allowing the use of off-the-shelf stereo models without additional training. Furthermore, we introduce a monocular cue-guided disparity refinement module to improve robustness across static and dynamic regions by incorporating monocular depth information from foundation models. Extensive experiments on real-world datasets demonstrate the superior zero-shot evaluation performance and enhanced generalization ability of our method compared to existing approaches.

1 Introduction

Stereo matching has witnessed significant advancements in recent years, driven by deep learning techniques and the availability of extensive training datasets in the image domain [18, 16, 20]. These advancements have enabled widespread applications in various fields, including mapping [10], navigation [21], 3D reconstruction [14, 9], motion estimation [7, 29], and image restoration [42, 19, 38]. Additionally, the abundance of unlabeled data on the internet has recently fueled the progress of monocular depth estimation [37, 25].

Event cameras report per-pixel relative intensity *changes* asynchronously at high temporal resolutions within a wide dynamic range [12], providing complementary sensory information alongside conventional frame-based cameras that capture *absolute* intensity values synchronously. Event-intensity asymmetric stereo matching has emerged as a promising approach to achieve robust performance in challenging conditions such as ultra-wide dynamic range and fast-moving scenes that cannot be faithfully captured by conventional frame-based cameras alone, by leveraging the complementary strengths of event and frame cameras in different views [30, 17, 46, 40, 4]. Despite the potential benefits, existing event-intensity asymmetric stereo approaches often rely on supervised learning or fine-tuning, requiring large amounts of labeled training data. Unfortunately, the shorter history of event-based sensors in commercial markets poses a scarcity of large-scale datasets essential for

[#] Equal contribution. [*] Corresponding author.

[1] Code available: https://github.com/HYLZ-2019/ZEST

38th Conference on Neural Information Processing Systems (NeurIPS 2024).

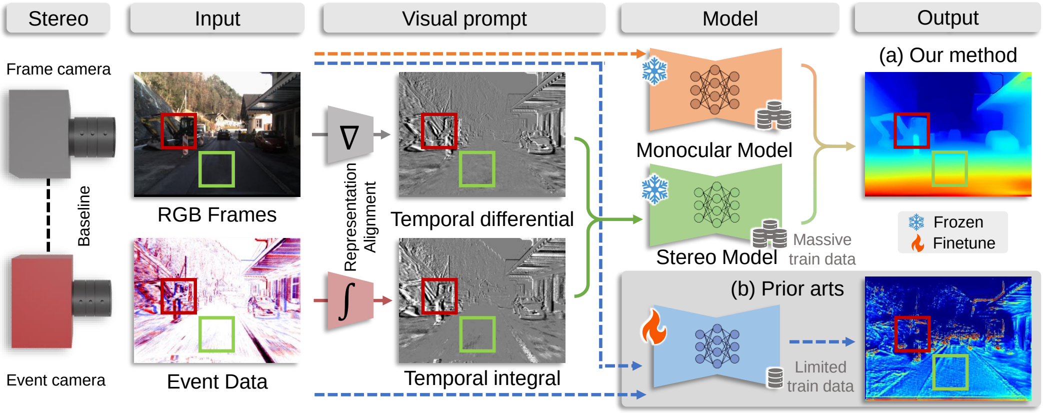

Figure 1: The proposed **Z**ero-shot **E**vent-intensity asymmetric **ST**ereo (ZEST) framework estimates disparity by finding correspondences between RGB frames and event data. (a) Our method conducts stereo matching by utilizing off-the-shelf stereo matching and monocular depth estimation models with frozen weights, and feeding them visual prompts tailored to the physical formulation of frames and events (temporal difference of frames and temporal integral of events, respectively). (b) In contrast, existing methods (*e.g.*, [40]) that rely on training data with known ground truth disparities often suffer from limited annotated data availability, thus leading to unsatisfactory results.

effective training and generalization. The scarcity of large-scale datasets in the event domain has resulted in overfitting and poor generalization to new environments or unseen disparity ranges [6].

Stereo models estimate disparity by establishing feature similarities between views, assuming that the two inputs are aligned in feature representation space. As events and frames capture relative differences and absolute values of intensity, respectively, they inherently possess a strong physical connection. This connection can be leveraged to convert them into intermediate representations with comparable appearance patterns. In the context of event-intensity asymmetric stereo, where training data are significantly limited compared to images, it is crucial and beneficial to develop a zero-shot approach that does not necessitate training data for modifying the underlying architecture or weights of the models. Considering the recent progress in image-based stereo matching [18, 16], where models trained on extensive datasets have exhibited effective zero-shot generalization, as well as the emerging techniques of "visual prompting" [32, 36, 1], which aims to adapt off-the-shelf models to new domains or modalities without modifying the model architecture or weights, we are motivated to utilize off-the-shelf models from the image domain with only modified inputs, rather than altering the weights, which requires substantial data.

Yet, several challenges impede the introduction of off-the-shelf models from the image domain to event in a zero-shot manner: 1) Significant modality gaps exist between events and frames (the red boxes in Figure 1), where events are triggered by temporal differences between frames exceeding predefined thresholds, compounded by sensor imperfections and stochastic electric noise. 2) In static regions where events cannot be triggered (the green boxes in Figure 1), no correspondences can be established, necessitating hallucination from the monocular model processing frames. However, these models typically provide relative disparities, whose distances from the actual metric are mostly calculated up to a global scale and bias.

In this paper, we propose a **Z**ero-shot **E**vent-intensity asymmetric **ST**ereo (ZEST) framework that leverages both monocular depth estimation and stereo matching models from the image domain, which is shown in Figure 1. To address the appearance gap between frames and events, we introduce a representation alignment module that considers the physical formulation from frames to events. The disparity map is then estimated from frames and events in different views using an off-the-shelf stereo model in the image domain. We further propose a monocular cue-guided disparity refinement module that re-renders these disparities by rescaling the relative depths predicted by a monocular depth estimation foundation model, enhancing robustness in regions with few events or textures. Our framework demonstrates superior performance among training-free methods for intensity-event asymmetric stereo matching and enhanced generalization across diverse real-world scenes. The

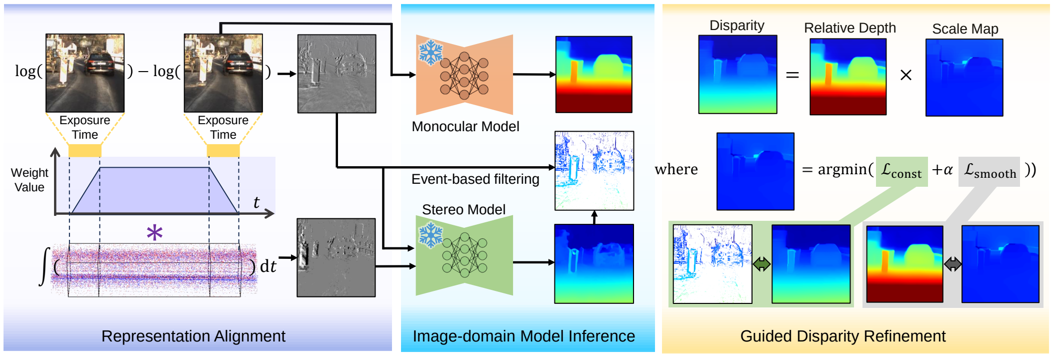

Figure 2: Overview of the proposed ZEST framework. The representation alignment module aligns frames and events, considering exposure time and event properties. This enables using an off-the-shelf stereo model to find correspondences. Disparity refinement then improves the estimates by minimizing differences between monocular depth prediction rescaled by an optimized scale map and binocular depth predictions, guided by event density confidence.

flexibility of our approach allows for seamless upgrades of the stereo and monocular models alongside advances in the related fields. Our main contributions are as follows:

- We present the first zero-shot event-intensity asymmetric stereo matching method that leverages off-the-shelf depth estimation models from the image domain.
- We introduce a visual prompting method for representation alignment between events and frames, enabling the utilization of off-the-shelf stereo models without modification.
- We propose a monocular cue-guided disparity refinement method for robustness in regions with few events or textures, inspired by recent advancements in monocular depth estimation.

2 Related Work

Intensity-based stereo and monocular depth estimation. With the development of deep learning technology, significant progress has been made in stereo matching, with methods categorized based on their cost construction and aggregation approaches. Correlation-based methods [27, 35, 39, 8] and those using 3D convolutions [3, 5, 33] have achieved impressive performance. Recently, iterative optimization-based networks [20, 34, 41] have demonstrated superior accuracy and robustness. In monocular depth estimation, models like Depth Anything [37] and MiDaS [25] leverage extensive unlabeled data to estimate relative depth, enabling generalization across domains at the cost of unknown scale and shift.

Event-based symmetric stereo. Event cameras capture pixel-level brightness changes asynchronously, offering advantages over conventional frame-based cameras. Event-based stereo depth estimation has emerged rapidly. Representative works include utilizing camera velocity [44] or estimating depth without explicit event matching [43]. Deep learning solutions have considered novel sequence embedding [28] and fusion of frame and event data [22, 23] for improved depth estimates in challenging scenarios. Recent efforts explore integrating off-the-shelf models from the image domain [6] to improve stereo matching performance by leveraging the inherent connection between frame and event data.

Event-intensity asymmetric stereo. Event-frame asymmetric stereo matching leverages the complementary strengths of event and frame cameras. Traditional methods focused on aligning and fusing asynchronous event data with synchronous frame data using hand-crafted features [17] and traditional stereo matching algorithms [30]. Deep learning approaches [46, 40, 4] have been employed to learn complex mappings for event-frame fusion and dense depth estimation. However, these methods often suffer from overfitting and poor generalization due to limited dataset sizes and scene diversity in the event domain. Our work proposes a zero-shot approach that leverages disparity estimation models from the image domain by visual prompting, eliminating the need for additional training and improving generalization.

3 Method

Overview The proposed method aims to estimate depth from a frame-based camera and an event camera in different views, separated by a baseline distance. Without loss of generality, we assume that the frames are in the left view and the events are in the right view. Given consecutive rectified event-intensity pairs $(I^{\mathrm{L}}(\tau_i), E^{\mathrm{R}}(\tau_i)$ and $(I^{\mathrm{L}}(\tau_{i+1}), E^{\mathrm{R}}(\tau_{i+1}))$, our goal is to infer the corresponding disparity map $D(\tau_i)$ at timestamp τ_i.

The overall framework of the proposed ZEST for event-intensity asymmetric stereo is shown in Figure 2, consisting of two components: the representation alignment module for aligning the frames in the left view and events in the right view into an intermediate representation space (Sec. 3.1), and the disparity refinement module for improving stereo matching results under the guidance of monocular model predictions (Sec. 3.2).

3.1 Event-intensity representation alignment for stereo matching

Stereo matching estimates depth by triangulation using pixel space representations, where stereo correspondence is established by finding similar patterns on a pixel-wise basis. With the advances in deep learning, modern stereo matching models are trained on massive data to estimate disparity. Due to the amount of training data and the diversity of real-world scenes, off-the-shelf models with frozen weights maintain robustness to different representations ranging from absolute values to relative changes in intensity, as shown in Figure 3. However, directly using these representations may not be optimal for event-intensity asymmetric stereo. This is because the event and frame data have fundamentally different characteristics, and a carefully designed intermediate representation can better bridge the appearance gap between them.

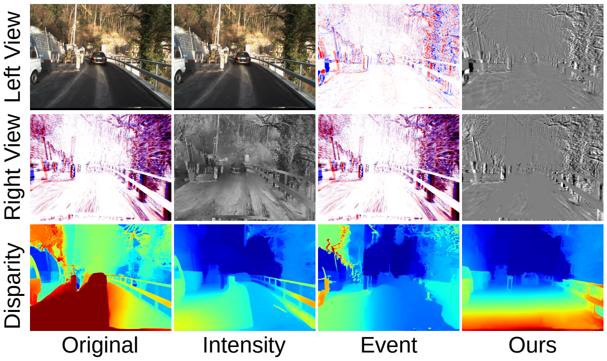

Figure 3: Visual comparisons of the disparity predicted by a stereo model [16] fed with inputs in the first two rows, where the inputs are aligned in the space of raw data, intensity (via [26]), events (via [15]), and intermediate (via the proposed method), respectively.

Inspired by this, we design an intermediate representation as a “visual prompt” to align the modalities in two views, enabling off-the-shelf stereo matching models to work for event-intensity asymmetric stereo. We will detail the formulation of the proposed intermediate representation in the following.

An event $e = (t, \boldsymbol{p}, \sigma)$ at the pixel $\boldsymbol{p} = (\boldsymbol{p}_x, \boldsymbol{p}_y)^\top$ and time t is triggered whenever the logarithmic change of irradiance I exceeds a pre-defined threshold c (> 0), *i.e.*,

$$\|\log I_{\boldsymbol{p}}(t) - \log I_{\boldsymbol{p}}(t - \Delta t)\| \geq c, \tag{1}$$

where $I(t)$ denotes the instantaneous intensity at time t, and the polarity $\sigma \in \{-1, +1\}$ indicates $\{$negative, positive$\}$ brightness changes. We define $e_{\boldsymbol{p}}(t)$ as a function of continuous time t such that,

$$e_{\boldsymbol{p}}(t) = \sigma \delta_\tau(t), \tag{2}$$

whenever there is an event $e = (\tau, \boldsymbol{p}, \sigma)$. Here, $\delta_\tau(t)$ is an impulse function, with unit integral, at time τ, and the sequence of events is turned into a continuous-time signal, consisting of a sequence of impulses. There is such a function $e_{\boldsymbol{p}}(t)$ for each position $\boldsymbol{p}$ in the image. Since each pixel can be treated separately, we omit the subscripts $\boldsymbol{p}$. Given a reference timestamp τ_i, assuming that there are latent sharp image sequences $I(\tau)$ with infinitesimal exposure time, their relationship between the corresponding events can be expressed as

$$I(\tau_{i+1}) = I(\tau_i) \exp\left(c \int_{\tau_i}^{\tau_{i+1}} e(t) dt\right). \tag{3}$$

Define the logarithmic brightness increment $\Delta L_i(t)$ from two consecutive frames as

$$\Delta L_i(t) = \log I(\tau_{i+1}) - \log I(\tau_i). \tag{4}$$

It can be approximated by events triggered during these frames as

$$\Delta \widehat{L}_i(t) = c \int_{\tau_i}^{\tau_{i+1}} e(t) dt. \tag{5}$$

In Eq. (5), the left-hand side represents the *temporal difference of frames*, while the right-hand side denotes the *temporal integral of events*. This formulation establishes an explicit intermediate representation that bridges the gap between frames and events with similar appearance, enabling correspondences to be found for stereo matching.

Now we turn to the frames captured in the real world, which have a non-negligible exposure time $2T$. A frame $I_{\tau,T}(t)$ with exposure time $[\tau - T, \tau + T]$ can be represented as the average of the latent image $I(t)$ over the exposure duration given a latent frame with a timestamp τ_0 as reference [24], which can be formulated as

$$I_{\tau,T}(t) = \frac{1}{2T} I(\tau_0) \int_{\tau-T}^{\tau+T} \exp\left(c \int_{\tau_0}^{t} e(s) ds\right) dt. \tag{6}$$

Then, the difference between two consecutive logarithmic frames $L_{\tau_i}, L_{\tau_{i+1}}$ with exposure time $2T$ with the middle latent frame I_{τ_0} as reference can be formulated as

$$\Delta \widehat{L}_i(t) = \log \left(\int_{\tau_i - T}^{\tau_i + T} \exp \left(c \int_{\tau_0}^{t} e(s) ds \right) dt \right) - \log \left(\int_{\tau_{i+1} - T}^{\tau_{i+1} + T} \exp \left(c \int_{\tau_0}^{t} e(s) ds) dt \right) \right). \tag{7}$$

We use the temporal difference map $\Delta L(t)$ defined by consecutive frames in Eq. (3) and its approximation version defined from the temporal integral of events in Eq. (7) as explicit intermediate representations, respectively. In practice, the calculations are done in discrete form, whose details can be found in the appendix. We normalize the event and image representations using percentile normalization to improve robustness.

Specifically, the disparity D^{bino} at timestamp t is estimated by stereo matching model $\mathcal{F}^{\text{bino}}$ as

$$D^{\text{bino}}(t) = \mathcal{F}^{\text{bino}}(\Delta L^{\text{L}}(t), \Delta \widehat{L}^{\text{R}}(t)). \tag{8}$$

As shown in Figure 3, the proposed event-intensity alignment method successfully finds appropriate visual prompts for the stereo models from the image domain, which helps to establish correspondences between the frames and events.

3.2 Monocular cue guided disparity refinement

In the context of event-intensity asymmetric stereo, stereo matching often faces challenges in establishing reliable correspondences, particularly in textureless regions of left images and static regions with sparse events in the right view. In contrast, monocular depth estimation directly infers depth maps from single images by leveraging monocular cues such as texture variations, gradients, occlusion, known object sizes, haze, and defocus. Off-the-shelf monocular depth estimation models, such as Depth Anything [37] and MiDaS [25], have demonstrated impressive "zero-shot cross-dataset transfer" capabilities, thanks to the relaxed requirements for training data in unsupervised learning.

Inspired by this, we propose a monocular cue-guided disparity refinement approach. However, there may be unknown scale and shift discrepancies between the predictions of the stereo and monocular models, which may vary spatially due to the absence of physically measurable information during monocular depth estimation. To address these factors, we model the desired refined disparity map as a locally linear transformation of the estimation from the monocular cue. Let D^{mono} represent the disparity map predicted by a monocular depth estimation model $\mathcal{F}^{\text{mono}}$ from frame I, *i.e.*,

$$D^{\text{mono}} = \mathcal{F}^{\text{mono}}(I), \tag{9}$$

whose relationship with the binocular estimation D^{bino} is assumed a linear transform as

$$D^{\text{bino}} \approx W \odot (D^{\text{mono}} + B), \tag{10}$$

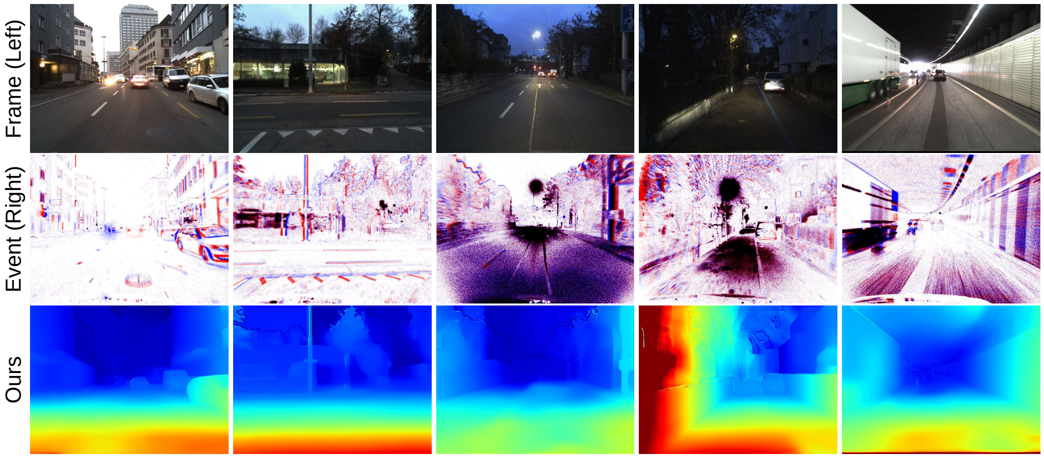

Figure 4: From left to right, our model exhibits impressive generalization abilities across a broad spectrum of varied scenes, encompassing sparse event scenes, richly textured environments, dimly lit settings, close-range captures, and high dynamic range situations.

where $\odot$ denotes the element-wise multiplication operation, and W and B denote the scale map and the shift map, respectively.

To estimate the scale map W and shift map B, we minimize the following loss function:

$$W^*, B^* = \operatorname{argmin}_{W,B} \mathcal{L}_{\text{const}} + \alpha \mathcal{L}_{\text{smooth}}, \tag{11}$$

where the loss function involves several priors about the desired disparity map, and α is a regularization parameter to balance between them. Note that D^{bino} is predicted by establishing correspondence between frames and events, which is more reliable where there are more events. Therefore, the temporal difference map $\Delta L^{\text{L}}(t)$ of frames is utilized to construct a confidence map C to identify the density of events. Firstly, the estimated scale map W and shift map B should be consistent with the model defined in Eq. (10), which can be constrained by

$$\mathcal{L}_{\text{const}} = \sum_{\boldsymbol{p}} \left| C_{\boldsymbol{p}}(W_{\boldsymbol{p}}(D^{\text{mono}}_{\boldsymbol{p}} + B_{\boldsymbol{p}}) - D^{\text{bino}}_{\boldsymbol{p}}) \right|, \tag{12}$$

where the ℓ_1 distance is utilized for its robustness to outliers. Secondly, the scales and biases for neighboring pixels should be similar, which can be derived by an edge-ware smoothness as

$$\mathcal{L}_{\text{smooth}} = \sum_{\boldsymbol{p}} \Big((|\partial_x W_{\boldsymbol{p}}| + |\partial_x B_{\boldsymbol{p}}|) e^{-\left(\partial_x D^{\text{mono}}_{\boldsymbol{p}}\right)^2} + (|\partial_y W_{\boldsymbol{p}}| + |\partial_y B_{\boldsymbol{p}}|) e^{-\left(\partial_y D^{\text{mono}}_{\boldsymbol{p}}\right)^2} \Big). \tag{13}$$

This regularizer encourages local smoothness in the scale and shift maps. To ensure stability in the optimization steps for only one sample, a good initialization is necessary. While the shift map B is simply initialized as all ones matrix $B^{(0)} = \mathbf{1}$, the scale map W is initialized as

$$W^{(0)} = \frac{\sum_{\boldsymbol{p} \in \Omega_{\boldsymbol{p}}} \left(C_{\boldsymbol{p}} D^{\text{bino}}_{\boldsymbol{p}} / (D^{\text{mono}}_{\boldsymbol{p}} + B^{(0)}_{\boldsymbol{p}}) \right)}{\sum_{\boldsymbol{p} \in \Omega_{\boldsymbol{p}}} C_{\boldsymbol{p}}}, \tag{14}$$

where $\Omega_{\boldsymbol{p}}$ is a window centered at position $\boldsymbol{p}$. This loss term ensures the consistency modeled in Eq. (10) in regions with more events measured by ΔL in the beginning of the optimization. At the end of the optimization, the refined disparity map $\widehat{D}$ can be obtained by

$$\widehat{D} = W^* \odot (D^{\text{mono}} + B^*). \tag{15}$$

The proposed method effectively combines the strengths of both stereo matching and monocular depth estimation, leveraging the accurate but sparse disparity estimates from stereo matching to guide the refinement of the dense but relative depth estimates from monocular depth estimation.

Table 1: Quantitative comparisons of disparity estimation results with state-of-the-art methods from both event and image domains. The end-point-error (EPE), root mean square error (RMSE), 3-pixel error (3PE, %), and 2-pixel error (2PE, %) are adopted for evaluation. Zu, In, and Th denote the Zurich City, Interlaken, and Thun sequences on the DSEC [13] dataset, respectively. Red and orange highlights indicate the first and second best performing technique for each metric. ↑ (↓) indicates that higher (lower) values are better. The method with a gray background is the only one that does not adhere to the cross-dataset evaluation protocol.

Method	EPE↓				RMSE↓				3PE↓				2PE↓			
	Zu	In	Th	All	Zu	In	Th	All	Zu	In	Th	All	Zu	In	Th	All
SHEF [30]	10.43	11.93	14.61	10.66	18.05	18.22	24.42	18.10	51.07	74.54	55.98	54.37	60.21	80.12	65.93	63.01
HSM [17]	8.65	8.34	8.42	8.60	19.11	17.96	19.16	18.95	32.55	36.40	30.87	33.08	42.10	45.77	38.15	42.60
DAEI [40]	12.43	12.09	13.89	12.39	15.66	15.44	17.12	15.63	87.10	86.02	89.97	86.96	91.48	90.74	93.58	91.39
DAEI [40]†	-	1.93	-	-	-	2.94	-	-	-	16.82	-	-	-	29.16	-	-
Translate event into intensity on the right view																
PSMNet-ETNet	29.58	30.27	19.68	29.64	44.80	44.67	34.23	44.74	80.09	85.98	75.93	80.90	89.33	91.95	87.14	89.69
CR-ETNet	27.99	19.20	5.25	26.67	34.31	26.93	12.31	33.19	31.90	25.44	12.75	30.92	40.46	35.64	20.42	39.71
DS-ETNet	20.84	24.04	2.93	21.22	29.32	40.45	5.67	30.78	34.19	36.18	23.00	34.42	43.46	47.43	33.10	43.98
PSMNet-E2VID	29.50	26.69	25.07	29.09	44.84	38.74	39.42	43.96	81.43	84.43	82.31	81.86	90.15	91.33	90.53	90.32
CR-E2VID	24.65	7.70	3.67	22.20	30.60	12.17	8.15	27.94	27.78	12.75	9.51	25.60	35.06	21.23	15.18	33.05
DS-E2VID	13.30	17.40	2.37	13.83	20.02	30.72	4.28	21.46	28.20	28.83	20.23	28.25	36.38	38.70	29.09	36.68
Translate intensity into event on the left view																
CFF-v2e	9.86	12.07	7.81	10.17	14.69	16.55	11.36	14.93	60.34	71.95	62.77	61.97	68.55	79.73	73.03	70.14
ZEST: Translate into intermediate representation on both views (Ours)																
Ours-CR-MiDaS	3.64	8.79	2.21	4.35	4.60	9.68	3.23	5.30	28.68	33.07	21.61	29.26	48.02	51.52	41.12	48.48
Ours-DS-MiDaS	2.24	7.66	1.68	3.00	3.46	12.07	2.82	4.66	14.48	17.57	12.46	14.91	26.31	28.58	22.39	26.61
Ours-CR-DA	3.18	9.00	1.31	3.99	4.27	9.93	2.40	5.05	9.75	10.48	7.26	9.84	18.76	18.05	14.23	18.64
Ours-DS-DA	2.24	7.66	1.71	2.99	3.44	12.05	2.86	4.64	14.67	17.44	13.11	15.05	26.14	28.21	22.83	26.41

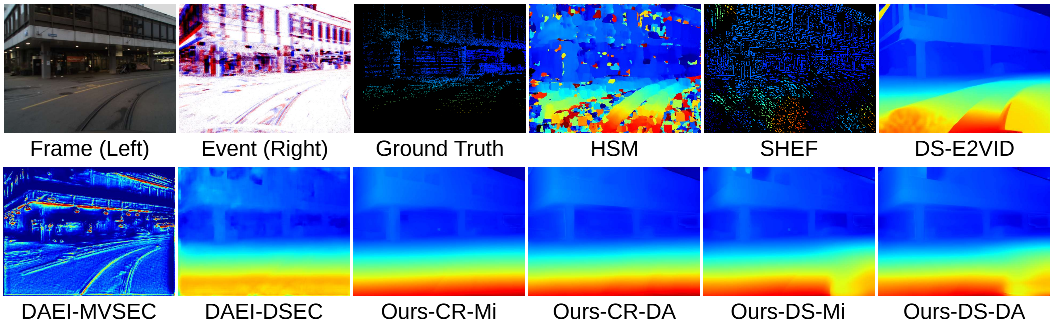

Figure 5: Visual quality comparison of disparity estimation results among state-of-the-art methods (HSM [17], SHEF [30], DAEI [40] trained on MVSEC [45] and DSEC [13], respectively) and the proposed ZEST with various stereo matching models (CR and DS) and monocular depth estimation models (Mi and DA). The baseline method with the best EPE and RMSE metrics, *i.e.*, DS-E2VID, is also included for comparison.

4 Experiments

Dataset. We evaluate the proposed ZEST framework on the widely-used benchmark dataset for event-intensity stereo matching, the DSEC dataset [13], a large-scale high-quality driving dataset with challenging scenes. It consists of synchronized event and frame streams captured from a stereo setup in a wider range of challenging scenarios, including fast motion, high dynamic range, and low light conditions. Specifically, it provides high-resolution (640 × 480) stereo event streams captured in outdoor driving scenes using Prophesee Gen 3.1 event cameras. It contains 53 driving scenarios taken in various lighting conditions. Without specification, all 41 sequences in the training set are adopted for evaluation. To demonstrate our method's generalization capabilities, we conduct additional evaluations on the MVSEC [45] and M3ED [2] datasets. MVSEC [45], the pioneering stereo event dataset, includes ground truth depth maps across diverse scenarios. It offers event streams at a spatial resolution of 346 × 260 captured with DAVIS346 event cameras. We use three subsets for MVSEC evaluation: indoor_flying1 (500–1500), indoor_flying2 (500–2000), indoor_flying3 (500-2500) (denoted as S1, S2, and S3, respectively). Since the image frame rate and ground truth

Table 2: Quantitative results of the proposed zero-shot disparity estimation method on the MVSEC [45] dataset.

Method	EPE↓				RMSE↓				3PE↓				2PE↓			
	S1	S2	S3	All	S1	S2	S3	All	S1	S2	S3	All	S1	S2	S3	All
HSM [17]	9.64	12.98	9.09	10.57	11.43	15.81	10.87	12.70	82.22	83.75	79.48	81.82	85.96	89.03	83.68	86.22
DAEI [40]	1.08	-	-	-	1.55	-	-	-	7.73	-	-	-	15.73	-	-	-
CR-E2VID	16.33	23.62	18.01	19.32	16.94	24.64	18.55	20.04	79.31	88.24	83.39	83.64	82.12	92.05	88.42	87.53
Ours-CR-DA	3.34	7.19	5.13	5.22	3.83	7.83	5.60	5.76	19.06	41.72	28.66	29.82	33.22	61.38	43.97	46.19

Table 3: Quantitative results of the proposed zero-shot disparity estimation method on the M3ED [2] dataset.

Method	EPE↓	RMSE↓	3PE↓	2PE↓
HSM [17]	12.39	14.27	90.87	92.58
DAEI [40]†	20.07	22.19	93.12	95.47
CR-E2VID	2.10	4.02	17.69	25.45
Ours-CR-DA	2.06	3.39	19.04	29.02

depth frame rate of MVSEC are different, for each frame we use the depth frame with the closest timestamp. The M3ED [2] dataset provides evaluation to unique urban and forest environments, providing high-resolution (1280 × 720) event streams captured with Prophesee EVK4 HD event cameras. We use the car_urban_day_horse (300-700) sequence for evaluation.

Metrics We use the standard evaluation metrics for stereo matching, including the mean absolute error (MAE), root mean squared error (RMSE), and the percentage of pixels with errors larger than a threshold (*e.g.*, 1, 2, or 3 pixels).

Compared methods. We compare the performance of the proposed ZEST framework with state-of-the-art event-intensity stereo matching methods, including both traditional and deep-learning-based approaches. For traditional methods, we consider SHEF [30] and HSM [17]. For deep-learning-based methods, we compare against a state-of-the-art method trained on the S2 and S3 splits of the MVSEC [45] dataset, DAEI [40]. A variant of DAEI trained on the Zurich and Thun sequences in the training set of DSEC [13] (denoted by DAEI†) is also included.

Baselines. We also include several baseline methods that directly apply the off-the-shelf stereo models to the event and frame images without extra representation alignment or disparity refinement. To align the different modalities between the left and right views, we consider two cases, event-to-intensity and intensity-to-event, respectively. In the case of event-to-intensity, events in the right view are reconstructed into a gray image using E2VID [26] and ETNet [31], which are then fed to the off-the-shelf image-based stereo models PSMNet [3], CREStereo (CR) [18], and DynamicStereo (DS) [16] together with the frames in the left view. In the case of intensity-to-event, consecutive frames in the left view are converted by v2e [15], which are then fed to the off-the-shelf event-based stereo models CFF [23] together with the events in the right view. As for the proposed ZEST framework, we adopt CR and DS for the stereo models, and Depth Anything (DA) [37] and MiDaS (Mi) [25] for the monocular depth estimation models, respectively. Throughout this paper, we use abbreviations to denote specific combinations of modality alignment techniques, stereo models, and monocular models. For example, the combination of the proposed technique, CREStereo, and Depth Anything is referred to as “Ours-CR-DA”. All results for comparison are produced from their official codes with recommended hyperparameters provided on public available sources or from the authors.

4.1 Comparisons with prior arts

Quantitative results on the benchmark dataset DSEC [13] are reported in Table 1, demonstrating the proposed method’s superior performance. The quantitative analysis revealed that our framework consistently outperformed almost all compared methods and baselines across every metric, except for DAEI† [40] and the baseline E2VID-CR. While all other methods are evaluated in a cross-dataset manner, DAEI† [40] is the only method that is evaluated in an in-dataset manner, which is trained and tested on the DSEC [13]. Therefore, it is not surprising that they achieve almost the best performance. Surprisingly, most of the variants of the proposed ZEST framework outperform this method in terms of 3PE metric, which demonstrates the effectiveness of the proposed method. The performance of the baseline CR-E2VID achieves good performance in terms of the 3PE and 2PE metrics in

Table 4: Quantitative results of ablation studies on the interlaken_00_c sequence of the DSEC [13] dataset. Compared to Table 1, 1-pixel error (1PE, %) is also utilized for evaluation.

Setting	Rep. alignment	Monocular cue	EPE↓	RMSE↓	3PE↓	2PE↓	1PE↓
1) DS w/ E2VID-right	✗	✗	43.02	55.79	87.63	91.57	95.98
2) DS w/ v2e-left	✗	✗	13.90	20.26	72.68	81.44	90.65
3) DS w/ spatial gradients	✗	✗	19.01	23.76	78.88	86.24	93.05
4) DS w/ spatial gradients + DA_Large	✗	✓	19.09	23.57	81.38	88.20	94.49
5) DA_Large	✗	✓	35.85	41.34	99.05	99.35	99.65
6) DA_Large w/ GT scale	✗	✓	2.40	3.16	28.35	47.45	72.07
7) Ours-DS w/o DA	✓	✗	1.49	2.85	7.77	16.84	47.84
8) Ours-DS-DA_Large	✓	✓	1.41	2.62	7.22	16.00	46.37
9) Ours-DS-DA_Base	✓	✓	1.39	2.59	6.96	15.60	46.17
10) Ours-DS-DA_Small	✓	✓	1.42	2.64	7.30	15.94	46.95

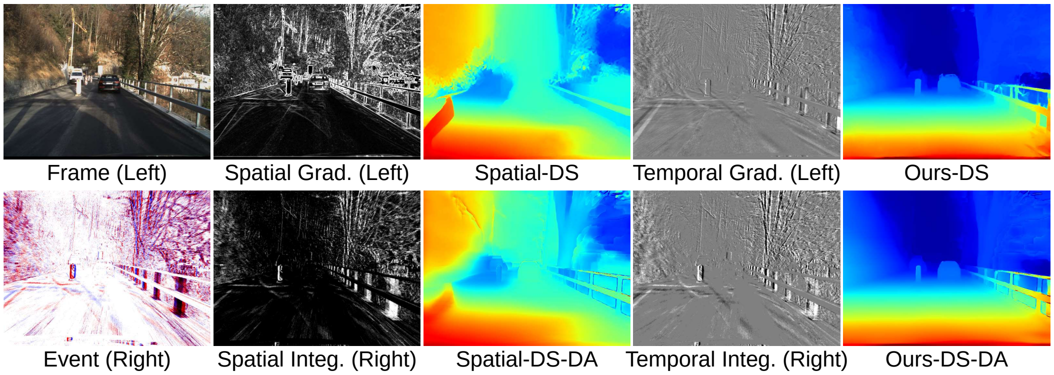
Frame (Left) Spatial Grad. (Left) Spatial-DS Temporal Grad. (Left) Ours-DS

Event (Right) Spatial Integ. (Right) Spatial-DS-DA Temporal Integ. (Right) Ours-DS-DA

Figure 6: Visual comparison of the disparity results of a stereo matching method DS using different representations and the proposed approach. From left to right: inputs, spatial gradients of frames and spatial integral of events (via [11]), their corresponding disparity result, the proposed representation, *i.e.*, the temporal difference of the frame and the temporal integral of the events, and their corresponding disparity result.

some sequences, although worse than the proposed method in all sequences. Evaluation results for MVSEC [45] and M3ED [2] datasets are shown in Tables 2 and 3, respectively. These results further confirm ZEST's robust generalization across diverse scenarios and its adaptability to varied environmental conditions.

The qualitative results presented in Figure 5 demonstrate the effectiveness of the proposed method. For the baselines, we include DS-E2VID [16], which achieved the best performance in terms of EPE and RMSE metrics. The visual comparisons highlight the superior quality of our framework, generating depth maps with significantly enhanced sharpness, intricate details, and improved dynamic accuracy compared to the compared methods.

4.2 Ablation study

To validate the effectiveness of each component in the proposed ZEST framework and analyze their contributions to the overall performance, we conduct a series of ablation studies to evaluate the impact of the representation alignment module and the monocular cue-guided disparity refinement module.

Impact of the representation alignment module. To assess the importance of the representation alignment module, we compare the performance of ZEST with and without this module. Quantitative results are shown in Table 4. In the absence of the proposed representation alignment, we feed the off-the-shelf stereo matching model DS with: 1) original frames and frames generated from events in the right view via E2VID (Figure 6); 2) events generated from frames in the left view via v2e and events in the right view; 3) the spatial gradient of frames in the left view and the spatial integral of events in the right view using [11]; and 7) the proposed representation alignment module. Among these settings, the proposed module achieves the best performance. This highlights the effectiveness of our approach in bridging the modality gap between events and frames, enabling the successful application of off-the-shelf stereo matching models. The corresponding qualitative results are shown in Figures 3 and 6, respectively.

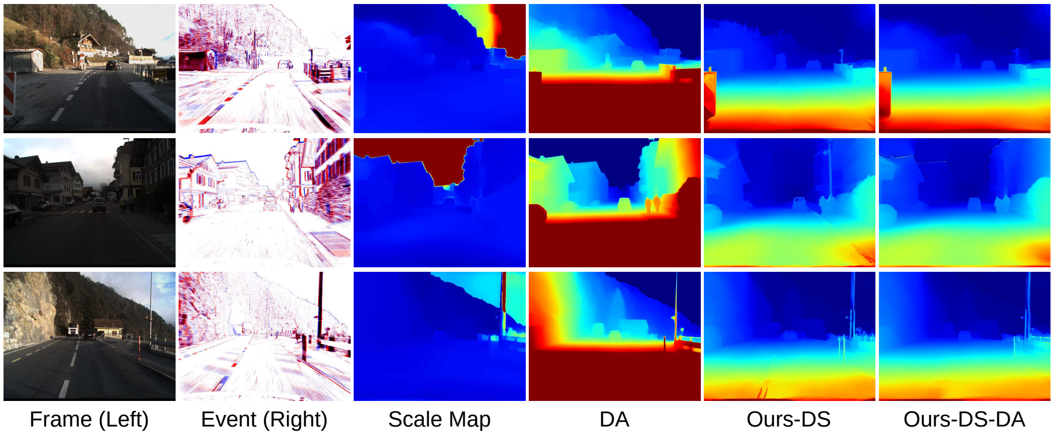

Figure 7: Visual comparison of the disparity results from the monocular model DA (fourth column), the proposed method without (fifth column), and with DA (last column), demonstrating the effectiveness of the proposed monocular cue-guided disparity refinement module. The corresponding optimized scale maps are shown in the third column.

Impact of the disparity refinement module. To validate the effectiveness of each component, we compare the proposed method with its five variants: 3) stereo matching model fed with the spatial gradient of frames in the left view and the spatial integral of events in the right view; 4) the results of 3) refined by a monocular depth estimation; 5) only the monocular depth estimation model DA; 6) the results of (5) rescaled by a global scale calculated from the ground truth disparity; 7) the proposed method without disparity refinement; and 8) the proposed method with DA for disparity refinement. The effectiveness of the introduction of monocular depth estimation can be shown by comparing 7) and 8) and the corresponding qualitative results are shown in Figure 7, whose results demonstrate more natural edges with DA. However, the disparity refinement module fails when the stereo matching results are totally not reliable, as shown in the comparison between 3) and 4). As shown in Figures 6 and 7, the disparity refinement module improves sharp depth boundaries for objects, such as cars, in challenging scenarios with sparse events or low-texture regions.

Impact of monocular depth estimation model size for refinement. The modular design of our framework supports flexible deployment with lighter-weight alternatives suited for resource-limited environments. While results in Table 1 employ the monocular depth estimation model DA_Large (335.3M parameters) with a ViT-L encoder, we also evaluated compact alternatives, DA_Base and DA_Small with 97.5M and 24.8M parameters, respectively, as detailed in 9) and 10) in Table 4. These alternatives provide substantial speed gains with acceptable accuracy trade-offs.

5 Conclusion

We introduce ZEST, a novel zero-shot event-intensity stereo matching framework that utilizes cutting-edge image domain models for accurate disparity estimation without training data. ZEST addresses the modality gap and labeled data scarcity in the event domain through representation alignment and monocular cue-guided disparity refinement. Experiments on DSEC show ZEST outperforms state-of-the-art methods in cross-dataset evaluation. Ablation studies validate the effectiveness of each component, highlighting the importance of representation alignment, model integration versatility, and monocular cue-guided refinement benefits.

Acknowledgments. This work was supported by National Natural Science Foundation of China (Grant No. 62136001, 62302019, 62088102, 62072188), Beijing Natural Science Foundation (Grant No. L233024), Beijing Municipal Science & Technology Commission, Administrative Commission of Zhongguancun Science Park (Grant No. Z241100003524012). Bin Fan was also supported by China Postdoctoral Science Foundation (Grant No. 2024M750101) and China National Postdoctoral Program for Innovative Talents (Grant No. BX20230013).

References

[1] Hyojin Bahng, Ali Jahanian, Swami Sankaranarayanan, and Phillip Isola. Exploring visual prompts for adapting large-scale models. *arXiv preprint arXiv:2203.17274*, 2022.

[2] Kenneth Chaney, Fernando Cladera, Ziyun Wang, Anthony Bisulco, M. Ani Hsieh, Christopher Korpela, Vijay Kumar, Camillo J. Taylor, and Kostas Daniilidis. M3ED: Multi-Robot, Multi-Sensor, Multi-Environment Event Dataset. In *Proc. of Computer Vision and Pattern Recognition Workshops*, pages 4015–4022, 2023.

[3] Jia-Ren Chang and Yong-Sheng Chen. Pyramid stereo matching network. In *Proc. of Computer Vision and Pattern Recognition*, 2018.

[4] Xihao Chen, Wenming Weng, Yueyi Zhang, and Zhiwei Xiong. Depth from asymmetric frame-event stereo: A divide-and-conquer approach. In *Proc. of Winter Conference on Applications of Computer Vision*, 2024.

[5] Xinjing Cheng, Peng Wang, and Ruigang Yang. Learning depth with convolutional spatial propagation network. *IEEE Transactions on Pattern Analysis and Machine Intelligence*, 42(10):2361–2379, 2020.

[6] Hoonhee Cho, Jegyeong Cho, and Kuk-Jin Yoon. Learning adaptive dense event stereo from the image domain. In *Proc. of Computer Vision and Pattern Recognition*, 2023.

[7] Bin Fan, Yuchao Dai, and Ke Wang. Rolling-shutter-stereo-aware motion estimation and image correction. *Computer Vision and Image Understanding*, 213:103296, 2021.

[8] Bin Fan, Ke Wang, Yuchao Dai, and Mingyi He. RS-DPSNet: Deep plane sweep network for rolling shutter stereo images. *IEEE Signal Processing Letters*, 28:1550–1554, 2021.

[9] Bin Fan, Yuchao Dai, Zhiyuan Zhang, and Ke Wang. Differential SfM and image correction for a rolling shutter stereo rig. *Image and Vision Computing*, 124:104492, 2022.

[10] Jorge Fuentes-Pacheco, José Ruiz-Ascencio, and Juan Manuel Rendón-Mancha. Visual simultaneous localization and mapping: A survey. *Artificial Intelligence Review*, 43(1):55–81, 2015.

[11] Guillermo Gallego, Henri Rebecq, and Davide Scaramuzza. A unifying contrast maximization framework for event cameras, with applications to motion, depth, and optical flow estimation. In *Proc. of Computer Vision and Pattern Recognition*, 2018.

[12] Guillermo Gallego, Tobi Delbruck, Garrick Michael Orchard, Chiara Bartolozzi, Brian Taba, Andrea Censi, Stefan Leutenegger, Andrew Davison, Jorg Conradt, Kostas Daniilidis, and Davide Scaramuzza. Event-based vision: A survey. *IEEE Transactions on Pattern Analysis and Machine Intelligence*, 44(1): 154–180, 2020.

[13] Mathias Gehrig, Willem Aarents, Daniel Gehrig, and Davide Scaramuzza. DSEC: A stereo event camera dataset for driving scenarios. *IEEE Robotics and Automation Letters*, 6(3):4947–4954, 2021.

[14] Leonardo Gomes, Olga Regina Pereira Bellon, and Luciano Silva. 3D reconstruction methods for digital preservation of cultural heritage: A survey. *Pattern Recognition Letters*, 50:3–14, 2014.

[15] Yuhuang Hu, Shih-Chii Liu, and Tobi Delbruck. v2e: From video frames to realistic dvs events. In *Proc. of Computer Vision and Pattern Recognition Workshops*, 2021.

[16] Nikita Karaev, Ignacio Rocco, Benjamin Graham, Natalia Neverova, Andrea Vedaldi, and Christian Rupprecht. DynamicStereo: Consistent dynamic depth from stereo videos. In *Proc. of Computer Vision and Pattern Recognition*, 2023.

[17] Haram Kim, Sangil Lee, Junha Kim, and H. Jin Kim. Real-Time Hetero-Stereo Matching for Event and Frame Camera With Aligned Events Using Maximum Shift Distance. *IEEE Robotics and Automation Letters*, 8(1):416–423, 2023.

[18] Jiankun Li, Peisen Wang, Pengfei Xiong, Tao Cai, Ziwei Yan, Lei Yang, Jiangyu Liu, Haoqiang Fan, and Shuaicheng Liu. Practical stereo matching via cascaded recurrent network with adaptive correlation. In *Proc. of Computer Vision and Pattern Recognition*, 2022.

[19] Jinxiu Liang, Yixin Yang, Boyu Li, Peiqi Duan, Yong Xu, and Boxin Shi. Coherent event guided low-light video enhancement. In *Proceedings of the IEEE/CVF International Conference on Computer Vision*, pages 10615–10625, 2023.

[20] Lahav Lipson, Zachary Teed, and Jia Deng. RAFT-Stereo: Multilevel recurrent field transforms for stereo matching. In *Proc. of International Conference on 3D Vision*, 2021.

[21] Daniel J. Mirota, Masaru Ishii, and Gregory D. Hager. Vision-based navigation in image-guided interventions. *Annual Review of Biomedical Engineering*, 13:297–319, 2011.

[22] Mohammad Mostafavi, Kuk-Jin Yoon, and Jonghyun Choi. Event-intensity stereo: Estimating depth by the best of both worlds. In *Proc. of International Conference on Computer Vision*, 2021.

[23] Yeongwoo Nam, Mohammad Mostafavi, Kuk-Jin Yoon, and Jonghyun Choi. Stereo depth from events cameras: Concentrate and focus on the future. In *Proc. of Computer Vision and Pattern Recognition*, 2022.

[24] Liyuan Pan, Richard Hartley, Cedric Scheerlinck, Miaomiao Liu, Xin Yu, and Yuchao Dai. High frame rate video reconstruction based on an event camera. *IEEE Transactions on Pattern Analysis and Machine Intelligence*, 44(5):2519–2533, 2020.

[25] René Ranftl, Katrin Lasinger, David Hafner, Konrad Schindler, and Vladlen Koltun. Towards robust monocular depth estimation: Mixing datasets for zero-shot cross-dataset transfer. *IEEE Transactions on Pattern Analysis and Machine Intelligence*, 44(3):1623–1637, 2022.

[26] Timo Stoffregen, Cedric Scheerlinck, Davide Scaramuzza, Tom Drummond, Nick Barnes, Lindsay Kleeman, and Robert Mahony. Reducing the sim-to-real gap for event cameras. In *Proc. of European Conference on Computer Vision*, 2020.

[27] Alessio Tonioni, Oscar Rahnama, Thomas Joy, Luigi Di Stefano, Thalaiyasingam Ajanthan, and Philip H. S. Torr. Learning to adapt for stereo. In *Proc. of Computer Vision and Pattern Recognition*, 2019.

[28] Stepan Tulyakov, Francois Fleuret, Martin Kiefel, Peter Gehler, and Michael Hirsch. Learning an event sequence embedding for dense event-based deep stereo. In *Proc. of International Conference on Computer Vision*, 2019.

[29] Ke Wang, Bin Fan, and Yuchao Dai. Relative pose estimation for stereo rolling shutter cameras. In *Proc. of International Conference on Image Processing*, 2020.

[30] Ziwei Wang, Liyuan Pan, Yonhon Ng, Zheyu Zhuang, and Robert Mahony. Stereo hybrid event-frame (SHEF) cameras for 3D perception. In *Proc. of International Conference on Intelligent Robots and Systems*, 2021.

[31] Wenming Weng, Yueyi Zhang, and Zhiwei Xiong. Event-based video reconstruction using Transformer. In *Proc. of International Conference on Computer Vision*, 2021.

[32] Chen Henry Wu, Saman Motamed, Shaunak Srivastava, and Fernando De la Torre. Generative visual prompt: Unifying distributional control of pre-trained generative models. In *Adv. of Neural Information Processing Systems*, 2022.

[33] Gangwei Xu, Junda Cheng, Peng Guo, and Xin Yang. Attention concatenation volume for accurate and efficient stereo matching. In *Proc. of Computer Vision and Pattern Recognition*, 2022.

[34] Gangwei Xu, Xianqi Wang, Xiaohuan Ding, and Xin Yang. Iterative geometry encoding volume for stereo matching. In *Proc. of Computer Vision and Pattern Recognition*, 2023.

[35] Haofei Xu and Juyong Zhang. AANet: Adaptive aggregation network for efficient stereo matching. In *Proc. of Computer Vision and Pattern Recognition*, 2020.

[36] Lingfeng Yang, Yueze Wang, Xiang Li, Xinlong Wang, and Jian Yang. Fine-grained visual prompting. In *Adv. of Neural Information Processing Systems*, 2023.

[37] Lihe Yang, Bingyi Kang, Zilong Huang, Xiaogang Xu, Jiashi Feng, and Hengshuang Zhao. Depth Anything: Unleashing the power of large-scale unlabeled data. In *Proc. of Computer Vision and Pattern Recognition*, 2024.

[38] Yixin Yang, Jin Han, Jinxiu Liang, Imari Sato, and Boxin Shi. Learning Event Guided High Dynamic Range Video Reconstruction. In *2023 IEEE/CVF Conference on Computer Vision and Pattern Recognition*, pages 13924–13934, 2023.

[39] Zhichao Yin, Trevor Darrell, and Fisher Yu. Hierarchical discrete distribution decomposition for match density estimation. In *Proc. of Computer Vision and Pattern Recognition*, 2019.

[40] Dehao Zhang, Qiankun Ding, Peiqi Duan, Chu Zhou, and Boxin Shi. Data association between event streams and intensity frames under diverse baselines. In *Proc. of European Conference on Computer Vision*, 2022.

[41] Haoliang Zhao, Huizhou Zhou, Yongjun Zhang, Jie Chen, Yitong Yang, and Yong Zhao. High-frequency stereo matching network. In *Proc. of Computer Vision and Pattern Recognition*, 2023.

[42] Changyin Zhou and Shree K. Nayar. Computational cameras: Convergence of optics and processing. *IEEE Transactions on Image Processing*, 20(12):3322–3340, 2011.

[43] Yi Zhou, Guillermo Gallego, Henri Rebecq, Laurent Kneip, Hongdong Li, and Davide Scaramuzza. Semi-dense 3D reconstruction with a stereo event camera. In *Proc. of European Conference on Computer Vision*, 2018.

[44] Alex Zihao Zhu, Yibo Chen, and Kostas Daniilidis. Realtime time synchronized event-based stereo. In *Proc. of European Conference on Computer Vision*, 2018.

[45] Alex Zihao Zhu, Dinesh Thakur, Tolga Ozaslan, Bernd Pfrommer, Vijay Kumar, and Kostas Daniilidis. The multi vehicle stereo event camera dataset: An event camera dataset for 3D perception. *IEEE Robotics and Automation Letters*, 3(3):2032–2039, 2018.

[46] Yi-Fan Zuo, Li Cui, Xin Peng, Yanyu Xu, Shenghua Gao, Xia Wang, and Laurent Kneip. Accurate depth estimation from a hybrid event-rgb stereo setup. In *Proc. of International Conference on Intelligent Robots and Systems*, 2021.

A Appendix

This appendix provides additional implementation details and extended experimental results for the ZEST framework introduced in the main paper. We aim to facilitate the reproducibility of our work and offer a more comprehensive analysis of the performance and robustness of ZEST under various conditions.

A.1 Implementation Details

Intermediate representation for stereo matching. Considering the physical formulation from frames to events, we design a representation that better captures the common information between the two modalities while suppressing their differences. Specifically, the proposed intermediate representation is designed to have the following properties: 1) It should be based on relative changes in intensity, which is the primary information captured by event cameras. 2) It should incorporate temporal information from the frames to match the temporal aggregation of events. 3) It should be robust to the different dynamic ranges and noise levels of event and frame data. By designing an intermediate representation with these properties, we aim to provide a more effective visual prompt for the off-the-shelf stereo matching models to adapt to the asymmetric characteristics of event and frame data. This can lead to an improved stereo matching performance in the event-intensity asymmetric setting compared to directly using the existing representations.

Now we provide the discrete form of the explicit representation defined in Eq. (7), which is used in practice since events with continuous time cannot be obtained. For convenience, we define the event map $E(t)$ as the integral of events between time τ and $\tau + \Delta\tau$ as $E_\tau(t)$ to represent the proportional change in intensity, which is equivalent to the sum of the polarity σ_k of the N_τ events $e_k = (t_k, \boldsymbol{p}, \sigma_k)$ at position $\boldsymbol{p}$ in discrete form:

$$E_\tau(t) = \int_{\tau}^{\tau+\Delta\tau} e(t)dt = \sum_{t_k \in [\tau, \tau+\Delta\tau]} \sigma_k. \tag{16}$$

Suppose that the duration of the exposure time $2T$ is discretized into N^{exp} temporal bins with a predefined unit duration $\Delta\tau$. By ignoring the logarithm effects of events, the temporal difference $\Delta L_i(t)$ between two consecutive frames $L_{\tau_i}, L_{\tau_{i+1}}$ can be expressed into a reweighted sum form of brightness increment $E(t)$ as

$$\Delta\widehat{L}_i(t) = c(\sum_{\tau=\tau_i+T}^{\tau_{i+1}-T} N^{\text{exp}} E_\tau + \sum_{\tau=\tau_{i+1}-T}^{\tau_{i+1}+T} \lfloor \frac{\tau_{i+1}+T-\tau}{\Delta\tau} \rfloor E_\tau - \sum_{\tau=\tau_i-T}^{\tau_i+T} \lfloor \frac{\tau-\tau_i+T}{\Delta\tau} \rfloor E_\tau), \tag{17}$$

where $\lfloor\cdot\rfloor$ denotes the round down operation. Note that, compared to the commonly used event-based double integral model [24] that uses trilateral weights to reweigh the event bin, the weights used in the proposed method are trapezoidal, as shown on the left of Figure 2, where the events during the readout time between frames are weighted equally according to the physical formulations. This new formulation is especially useful when neither the exposure phase nor the readout phase is negligible towards each other.

In real scenarios, the event trigger threshold c is often unknown. However, Eq. (17) still holds after we normalize both sides of the equation, which eliminates the unknown c.

In summary, we use the temporal difference map $\Delta L(t)$ defined by consecutive frames in Eq. (3) and its approximation version defined from the temporal integral of events in Eq. (17) as explicit intermediate representations, respectively.

Loss minimization in disparity refining. To estimate the scale map and shift map used for disparity refining, we minimize the loss function in Eq. (11). We perform this minimization using the gradient descent algorithm, implemented with PyTorch and the Adam Optimizer. For each image, we run the optimizer for 500 iterations.

Experimental setup. All models are tested on a single NVIDIA RTX 4090 GPU. The representation alignment algorithm and the disparity refining algorithm are capable of running on either a CPU or GPU, while the off-the-shelf stereo and monocular depth estimation models require GPU acceleration.

Table 5: Computational complexity breakdown per stage. Runtime (ms), GPU memory usage (MB), number of parameters (M), and equivalent FPS are reported.

Stage	Memory	Params	Runtime	FPS
Representation	0	–	39.06	25.59
DS	9224	21.47	8515.32	0.11
CR	2078	5.43	243.55	4.11
DA	3640	335.32	79.99	12.5
MiDaS	3344	344.05	31.14	32.10
Refinement	1736	–	306.82	3.25

Table 6: Computational complexity analysis across methods. 3PE performance, runtime (ms), GPU memory usage (MB), number of parameters (M), and equivalent FPS are reported.

Method	3PE↓	Memory	Params	Runtime	FPS
SHEF [30]	54.37	0	–	28944.85	0.03
HSM [17]	33.08	766	–	224.85	4.44
DAEI [40]	86.96	3238	11.25	75.15	13.3
Ours-DS-DA	15.05	14600	356.79	8902.13	0.11
Ours-DS-MiDaS	14.91	14304	365.52	8853.27	0.11
Ours-CR-DA	9.84	7454	340.75	630.36	1.58
Ours-CR-MiDaS	29.26	7158	349.48	581.51	1.71

Off-the-shelf model usage. In our experiments, we use stereo models PSMNet [3], CREStereo (CR) [18], and DynamicStereo (DS) [16]. For PSMNet, we use the officially released checkpoint trained on KITTI2015. For CR, we use the non-official implementation on `https://github.com/ibaiGorordo/CREStereo-Pytorch`, which is converted from the original MegEngine implementation. For DS, we use the pretrained model trained on both DynamicReplica and SceneFlow. The monocular depth estimation models we used are DepthAnything (DA) [37] and MiDaS (Mi) [25]. For DA, we use the pretrained model Depth-Anything-Large, which has 335.3M parameters. For Mi, we use the the pretrained model BEiT-L-512 of MiDaS 3.1, which has 345M parameters.

Evaluation dataset. In the experiments, we use the “train" split of the DSEC dataset for evaluation, as ground truth disparity is not provided for the official “test" split. The train split has 41 sequences, including 5 Interlaken sequences, 1 Thun sequence, and 35 Zurich City sequences. As some of the compared methods have border problems, for example, E2VID cannot reconstruct the first frame since there are no events recorded before $t = 0$, we exclude the results of the first 10 frames and the last 10 frames of each sequence when calculating metrics.

DAEI finetuning. The original DAEI [40] model was trained on MVSEC, and cannot generalize to the DSEC dataset. We finetuned it on DSEC, using the Thun and Zurich City sequences, and tested it on the Interlaken sequences. We trained on a single NVIDIA RTX 4090 GPU for 34 epochs until the metrics converged.

A.2 More Qualitative Results

We provide additional qualitative comparisons of the disparity estimation results obtained by ZEST and state-of-the-art methods on the DSEC [13] dataset. The qualitative results of the baseline methods are shown in Figure 8 and Figure 9. Qualitative results of our methods and the compared methods are shown in Figure 10 and Figure 11. More qualitative results of the representation alignment method are shown in Figure 12. More intermediate results of the disparity refining method are shown in Figure 13. More results on diverse real-world scenes of our method are shown in Figure 14. The qualitative results of the proposed method on the MVSEC [45] and M3ED [2] datasets are shown in Figures 15 and 16.

A.3 Computational Efficiency

We evaluated the computational efficiency of our framework's modules on a machine with an Intel i7-13700K CPU and NVIDIA RTX 4090 GPU, using an input resolution of 480×640. Unless noted otherwise, performance metrics were derived from the interlaken_00_c sequence from the DSEC dataset. Table 5 provides a breakdown of the computational cost per algorithm stage. The Ours-CR-DA variant achieves an average runtime of 630.36 ms per frame, consuming 7454 MB of

Table 7: Disparity refinement module computational cost across different iterations. EPE and 3PE performance, runtime (ms), and equivalent FPS are reported.

Iterations	EPE↓	3PE↓	Runtime	FPS
0	1.487	7.785	4.20	238.06
50	1.488	8.028	42.39	23.59
100	1.451	7.457	70.92	14.10
200	1.430	7.270	127.75	7.82
300	1.420	7.234	188.14	5.31
400	1.413	7.227	247.63	4.03
500 (Ours)	1.409	7.230	306.82	3.25

Table 8: Computational cost comparison at different input resolutions, reporting runtime (ms) and GPU memory usage (MB).

Input	CRES		DA		Refinement	
	Runtime	Memory	Runtime	Memory	Runtime	Memory
240×320 (1×)	156.59	2064	81.27	3640	300.96	1688
480×640 (4×)	243.55	2078	80.00	3640	306.82	1736
720×960 (9×)	624.11	2738	80.26	3640	311.70	1808

GPU memory. The disparity refinement module is the most computationally intensive component, representing 48.6% of the total runtime. In the Ours-DS-DA variant, the DS model accounts for most of the computational load, while the DA and refinement modules add minimal additional overhead. In Table 6, we compare the total computational cost of existing methods and the proposed one.

Profiling results in Table 7 indicate that the disparity refinement module requires approximately 306.82 ms, or 48.6% of the Ours-CR-DA variant's total inference time (630.36 ms). This module's overhead can be reduced without significantly impacting performance by limiting the number of iterations.

We also evaluated the scalability of our approach with varying input resolutions. As illustrated in Table 8, GPU memory usage and runtime increase marginally with larger resolutions. This is primarily due to the DA model, which internally operates at a fixed inference resolution, keeping memory usage stable.

A.4 Limitations

Despite the impressive performance of ZEST in event-intensity asymmetric stereo matching, there remain several limitations that warrant further investigation.

One challenge is handling noisy or sparse events, which can diminish the accuracy of visual prompts and stereo matching. In cases of poor event data quality, such as significant noise or low event density, the disparity refinement module may struggle to compensate, resulting in suboptimal depth estimation. Representative failure cases are illustrated in Figure 17. Row 1 shows the impact of noisy events on visual prompts, where noise increases the visual discrepancy between views. While the stereo model manages these inconsistencies effectively in most cases (*e.g.*, Rows 1 & 2), occasional failures occur. In Row 1, the CR stereo model produced errors, with the monocular DA predictions partially refining the disparity estimate. However, the final outcome remained suboptimal. Row 2 depicts the impact of sparse events, where the limited event information was insufficient for accurate stereo matching, and the refinement module struggled to compensate.

Additionally, The representation alignment module employed in the current framework relies on a fixed transformation, which may not fully capture the intricacies of the modality gap between events and frames. Future research could explore more expressive modality alignment techniques, such as learning-based approaches or domain adaptation methods, to improve the robustness and generalization capabilities of the framework.

Furthermore, while we demonstrate ZEST using off-the-shelf image-domain models, their large parameter counts contribute to a high computational load during inference. Nevertheless, ZEST's modular design allows for lightweight alternatives to be substituted in place of the stereo and monocular depth estimation models. This flexibility provides options for resource-limited deployments, albeit with some trade-offs in accuracy.

A.5 Broader Impacts

The proposed ZEST framework has the potential to significantly advance the field of event-intensity asymmetric stereo matching and enable a wide range of applications in various domains. In autonomous driving, the improved disparity estimation provided by ZEST can contribute to better obstacle detection, 3D object location, and scene understanding, ultimately improving the safety and reliability of self-driving vehicles. In robotics, the enhanced depth perception enabled by our method can facilitate more precise object manipulation, navigation, and mapping tasks, particularly in dynamic environments where conventional frame-based cameras may struggle. Furthermore, the zero-shot learning approach of ZEST lowers the entry barrier for researchers and practitioners to explore the benefits of event-intensity asymmetric stereo matching in their specific fields, as it eliminates the need for large-scale labeled training data.

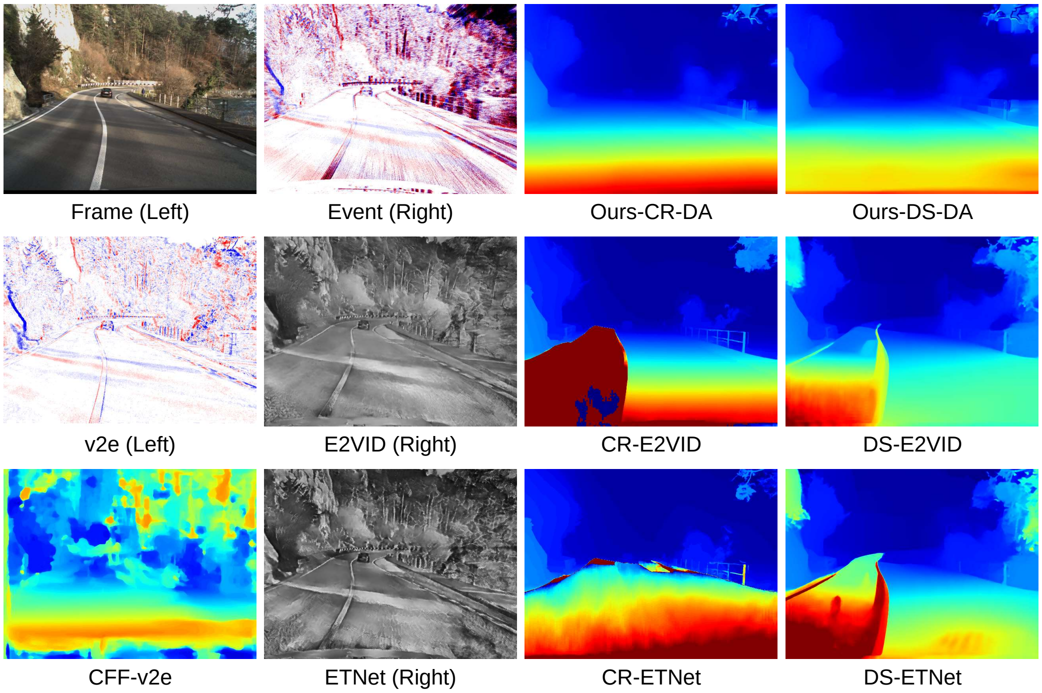

Frame (Left) | Event (Right) | Ours-CR-DA | Ours-DS-DA

v2e (Left) | E2VID (Right) | CR-E2VID | DS-E2VID

CFF-v2e | ETNet (Right) | CR-ETNet | DS-ETNet

Figure 8: Qualitative comparison of our method and baseline methods. Our methods demonstrate better robustness.

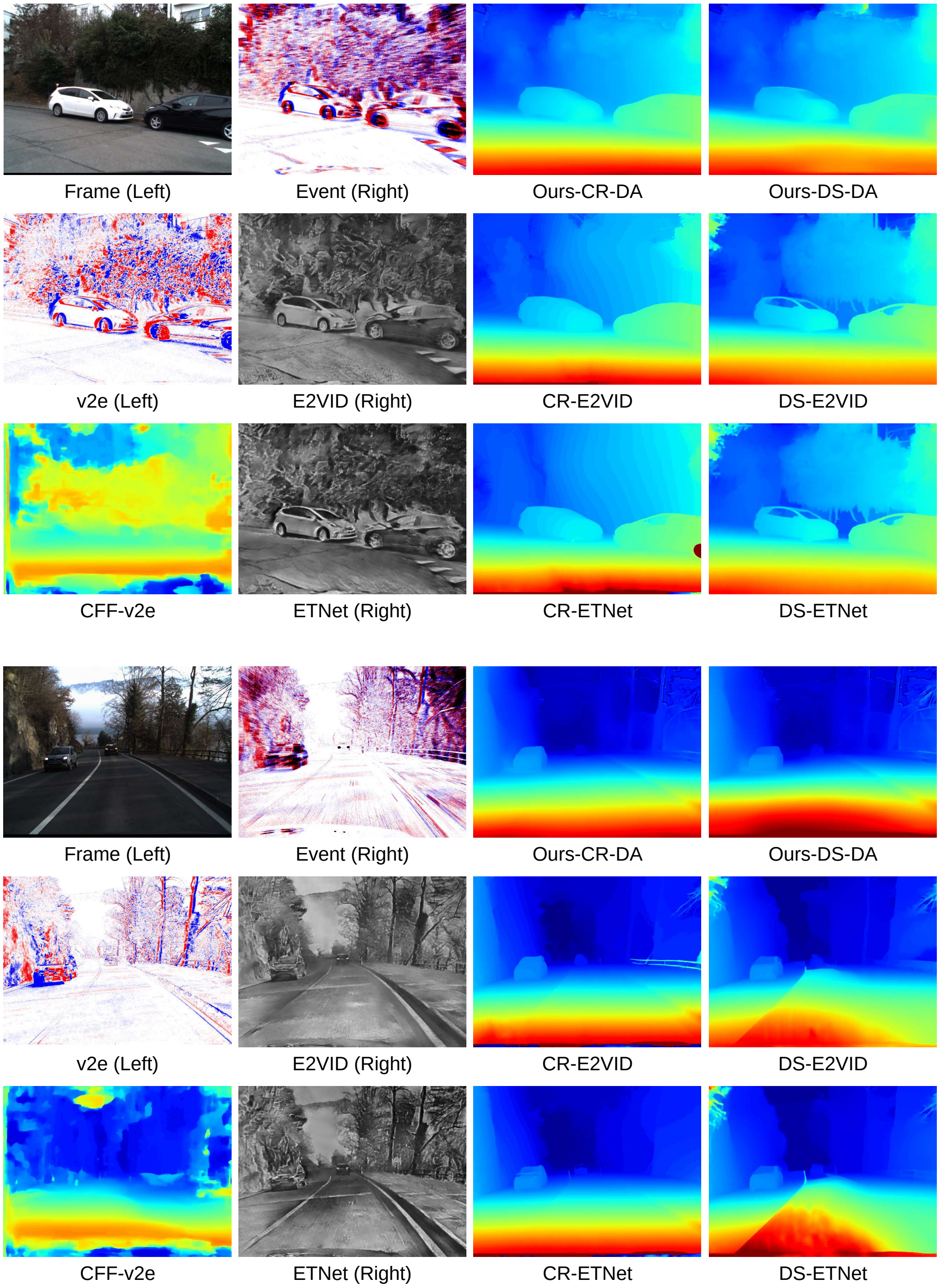

Frame (Left) Event (Right) Ours-CR-DA Ours-DS-DA

v2e (Left) E2VID (Right) CR-E2VID DS-E2VID

CFF-v2e ETNet (Right) CR-ETNet DS-ETNet

Frame (Left) Event (Right) Ours-CR-DA Ours-DS-DA

v2e (Left) E2VID (Right) CR-E2VID DS-E2VID

CFF-v2e ETNet (Right) CR-ETNet DS-ETNet

Figure 9: Qualitative comparison of our method and baseline methods. Our methods demonstrate better robustness.

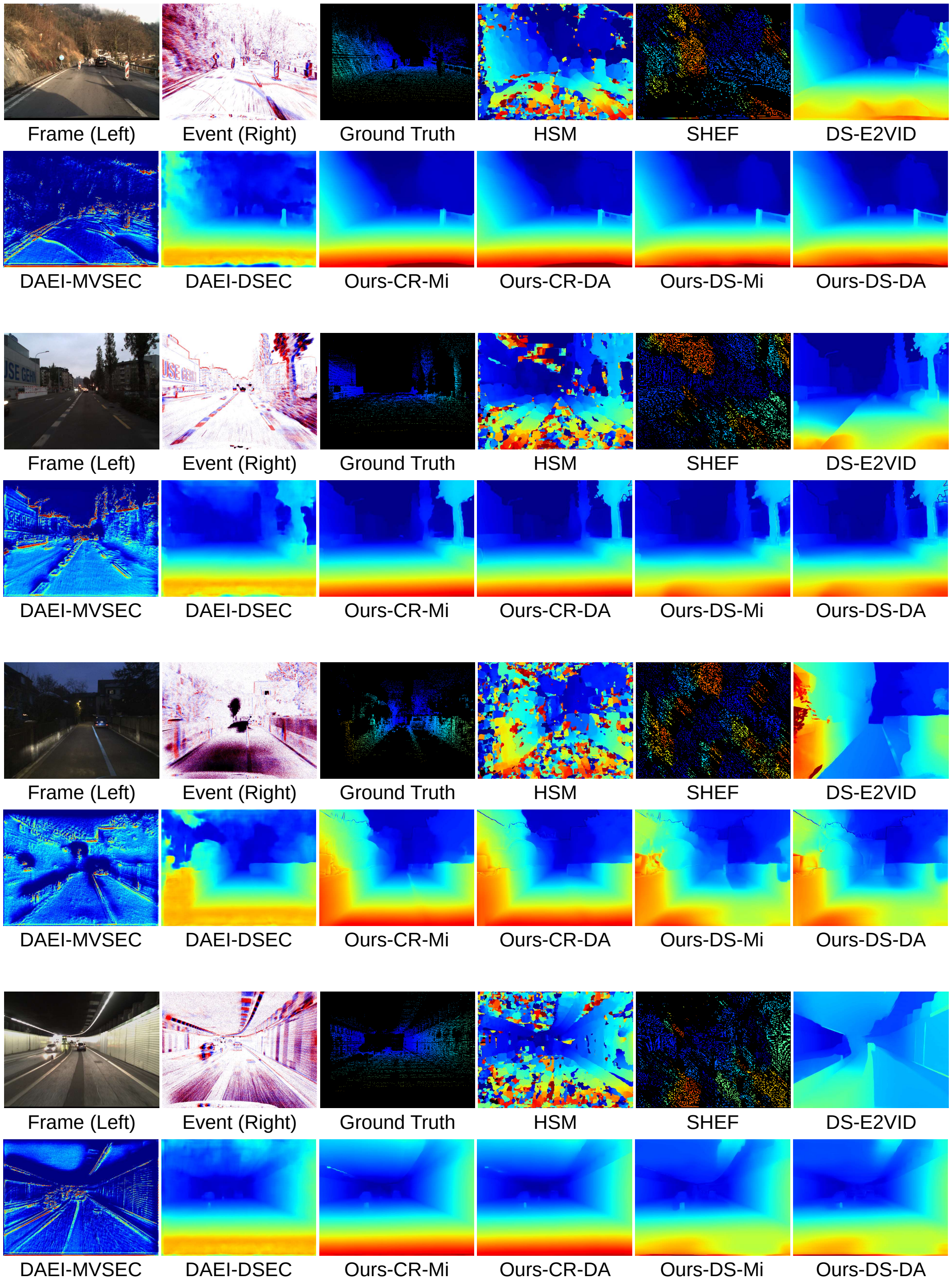

Figure 10: Qualitative comparison of our method and other methods.

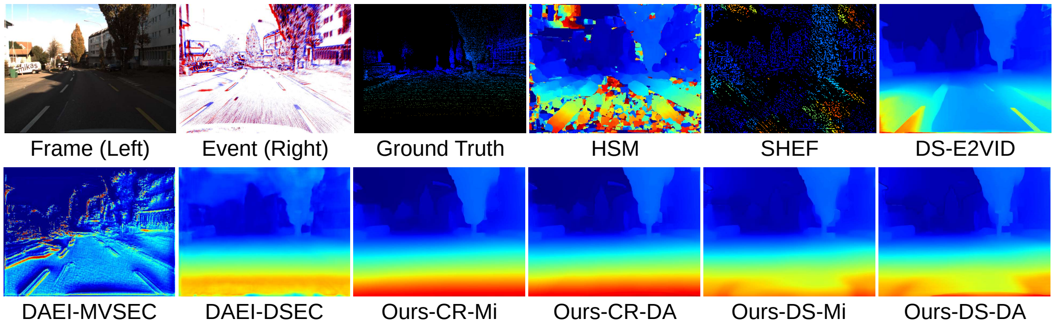

Figure 11: Qualitative comparison of our method and other methods.

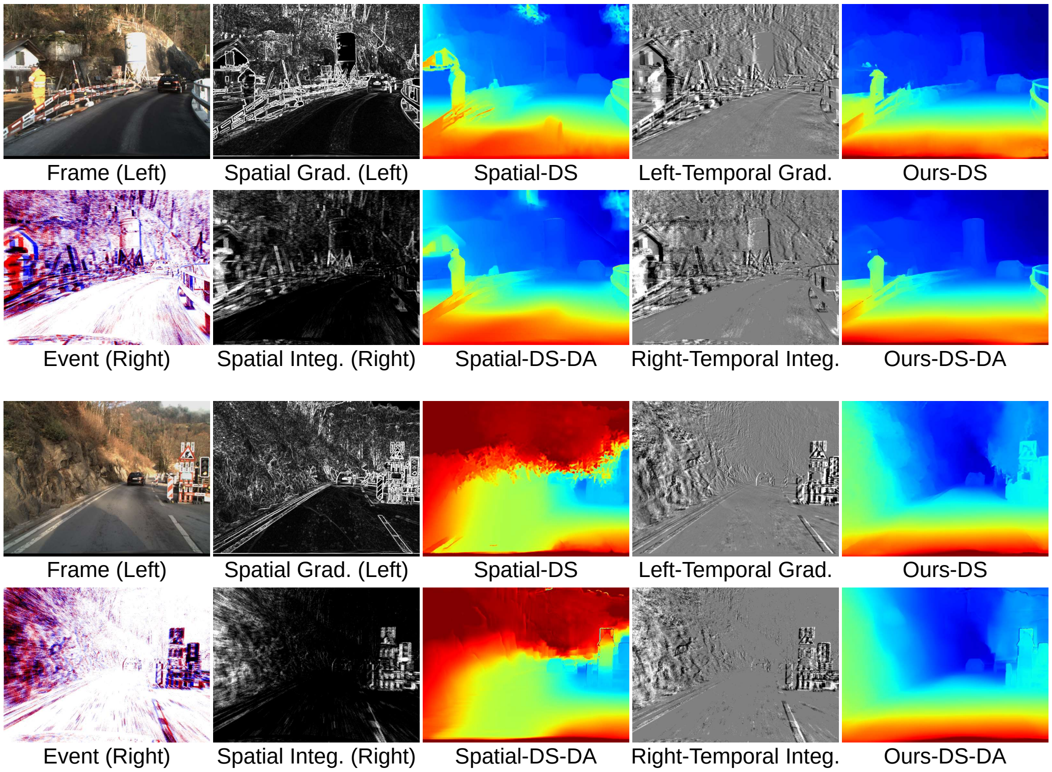

Figure 12: Qualitative comparison of our method and other representations.

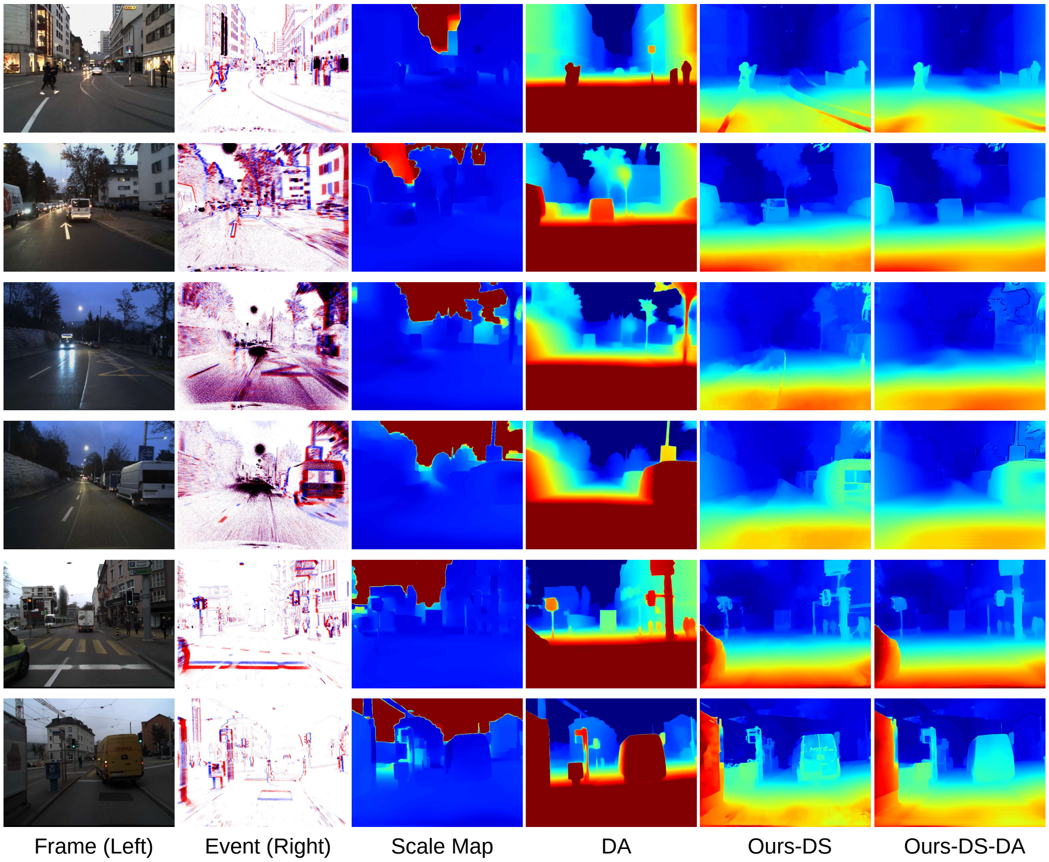

Figure 13: Intermediate results of disparity refining.

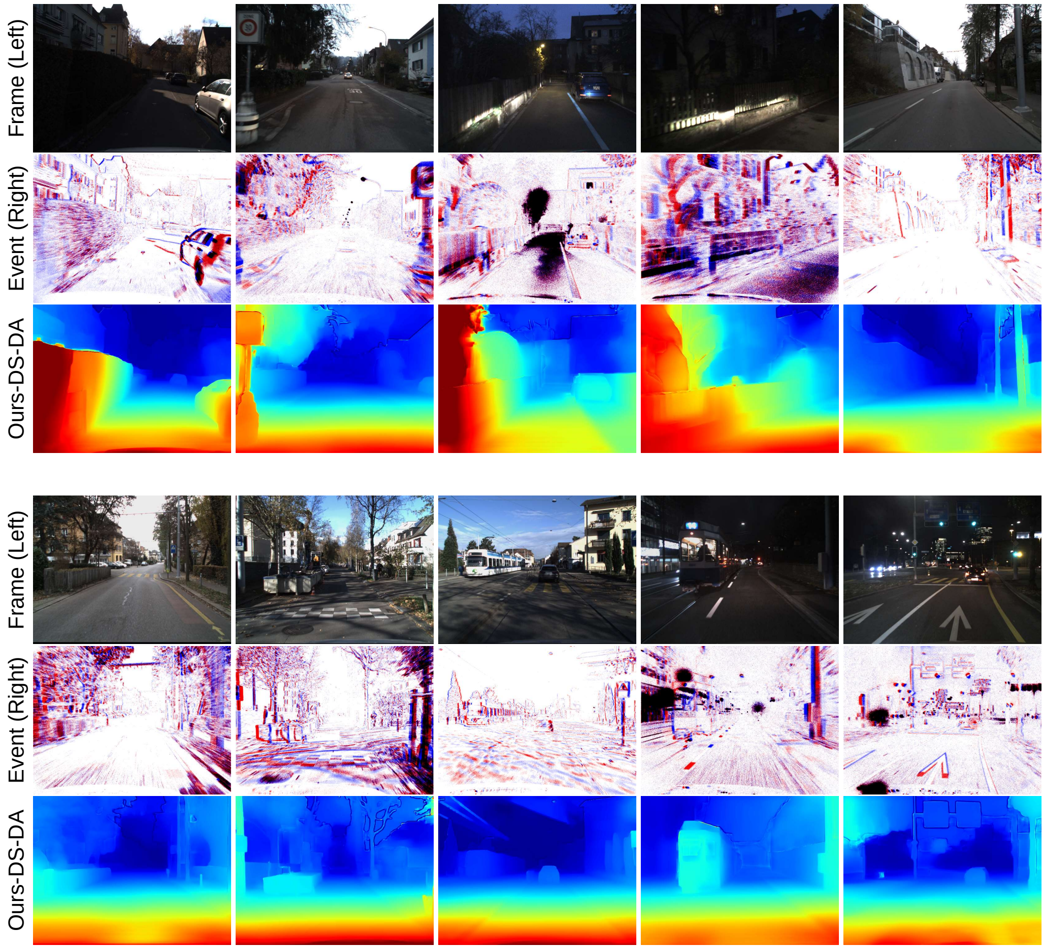

Figure 14: Results of our method in diverse scenarios.

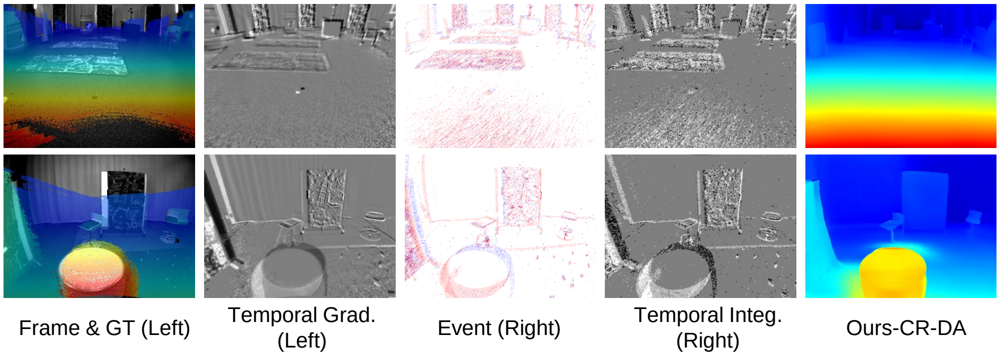

Figure 15: Comparison of disparity estimation results for real data from the indoor_flying1 sequence of the MVSEC [45] dataset.

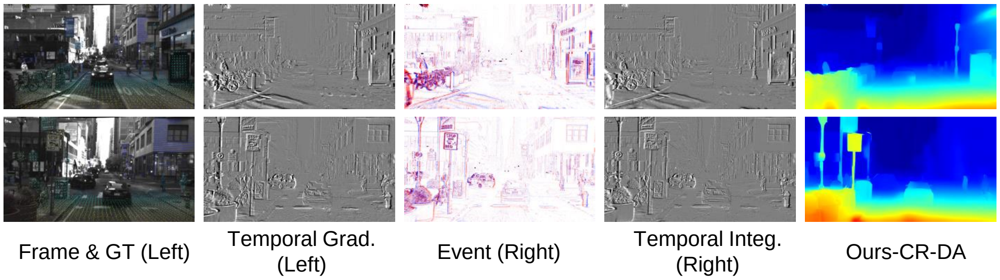

Figure 16: Comparison of disparity estimation results for real data from the car_urban_day_horse sequence of the M3ED [2] dataset.

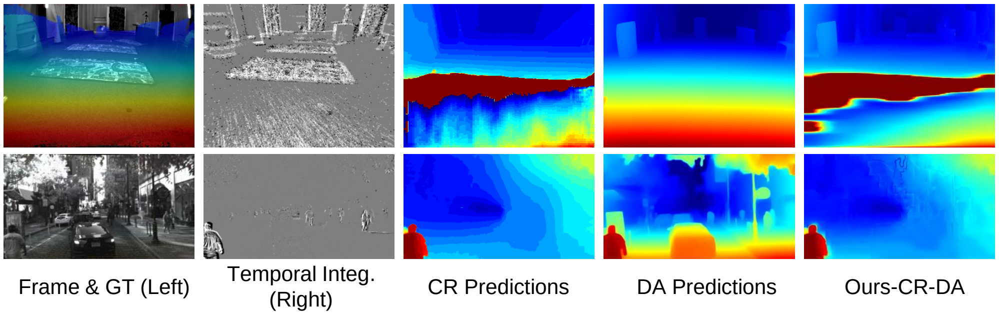

Figure 17: Examples of failure cases for the proposed method.